



UNIVERSITY OF LEEDS

This is a repository copy of *Highly Selective Catalysis at the Liquid–Liquid Interface Microregion*.

White Rose Research Online URL for this paper:
<https://eprints.whiterose.ac.uk/170100/>

Version: Accepted Version

Article:

Zhang, Y, Ettelaie, R orcid.org/0000-0002-6970-4650, Binks, BP et al. (1 more author)
(2021) Highly Selective Catalysis at the Liquid–Liquid Interface Microregion. ACS Catalysis, 11. pp. 1485-1494. ISSN 2155-5435

<https://doi.org/10.1021/acscatal.0c04604>

© 2021 American Chemical Society. This is an author produced version of an article published in ACS Catalysis. Uploaded in accordance with the publisher's self-archiving policy.

Reuse

Items deposited in White Rose Research Online are protected by copyright, with all rights reserved unless indicated otherwise. They may be downloaded and/or printed for private study, or other acts as permitted by national copyright laws. The publisher or other rights holders may allow further reproduction and re-use of the full text version. This is indicated by the licence information on the White Rose Research Online record for the item.

Takedown

If you consider content in White Rose Research Online to be in breach of UK law, please notify us by emailing eprints@whiterose.ac.uk including the URL of the record and the reason for the withdrawal request.



eprints@whiterose.ac.uk
<https://eprints.whiterose.ac.uk/>

Highly Selective Catalysis at the Liquid-Liquid Interface Micro-Region

Yabin Zhang¹, Rammile Ettelaie², Bernard P. Binks³, and Hengquan Yang^{1*}

¹ School of Chemistry and Chemical Engineering, Shanxi University, Taiyuan 030006, China

² Food Colloids Group, School of Food Science and Nutrition, University of Leeds, Leeds LS2 9JT, UK

³ Department of Chemistry and Biochemistry, University of Hull, Hull. HU6 7RX, UK

Supporting Information

ABSTRACT: Liquid-liquid interfaces in principle have the potential to regulate the selectivity of chemical reactions because of highly anisotropic microenvironments, but have not yet been well exploited. Here, we present a liquid-liquid interface-based strategy to boost catalytic selectivity, exemplified by selective hydrogenation of α,β -unsaturated aldehydes. The key to this success is the spatially controlled assembly of tubular catalyst particles just at the narrow inner interfacial layer of Pickering emulsion water droplets. The catalyst particles that are assembled at the inner interfacial layer of water droplets exhibit much higher selectivity to C=O hydrogenation than ones located either at the outer interfacial layer, in the interior of droplets or at the conventionally-called Pickering emulsion interface. 92.0–98.0% selectivity to the thermodynamically and kinetically unfavorable C=O hydrogenation over the C=C hydrogenation was achieved unexpectedly. Our strategy and the phenomena of interfacial catalysis reported here constitute an important supplement to the existing methods for the tuning catalytic selectivity, providing tremendous opportunities to construct highly selective catalysis systems.

KEYWORDS: biphasic catalysis; Pickering emulsions; liquid/liquid interface; heterogeneous catalysis

1. INTRODUCTION

To improve catalytic selectivity is a long-standing theme for chemical synthesis.^{1,2} A typical example is the selective hydrogenation of α,β -unsaturated aldehydes to unsaturated alcohols, obtaining important industry-relevant intermediates. This transformation is always known as a challenging reaction because the desired hydrogenation of the C=O bond is, however, thermodynamically and kinetically unfavorable over the C=C bond.^{3,4} To improve the selectivity to the C=O hydrogenation, several catalysts have been developed such as organic molecule-modified metal nanoparticles,^{5–8} metal-supported catalysts,^{9–16} bimetallic catalysts,^{17–19} and organometallic catalysts.²⁰ Despite state-of-the-art progress made and cutting-edge catalysis knowledge obtained, these methods of selectivity regulation are largely limited to the tuning of electronic state and structure of catalysts.

Liquid-liquid interface is ubiquitous chemical reaction systems. This kind of interface in principle has the potential to regulate the selectivity of chemical reactions because they feature anisotropy of a few nanometers thickness,^{21,22} interfacial acidity-basicity,²³ and unique

interfacial microenvironments.^{24,25} Past two decades witnessed that amphiphilic molecular catalysts or solid particle catalysts were assembled at the liquid-liquid interfaces for catalytic reactions, leading to high selectivity.^{26–35} For example, enantio-selectivity significant enhancement was observed when amphiphilic molecular catalysts were assembled at the liquid-liquid interfaces through formation of emulsions or micelles.^{26–28} Solid particle catalysts were also assembled at the liquid-liquid interfaces through the Pickering emulsion (solid particle-stabilized emulsion) effects.^{29–41} One noteworthy finding for the catalysis at Pickering emulsion interfaces is that the selectivity of cascade reaction was improved due to the phase-selective partitioning of reactants in a biphasic system.^{29,34} Although tremendous progress made, harnessing the aforementioned salient features of the liquid-liquid interfaces to tune catalytic selectivity has not yet been well explored so far. The main reason for this obstacle is that the catalyst at the liquid-liquid interface protrudes partly into the oil phase (organic phase) and partly into the water phase, which is true especially for particle catalysts.^{29–33} Consequently, it is practically difficult to precisely control the reaction solely at the narrow

interfacial layer of aqueous side or oil side. Janus particles that consist of a hydrophobic part and a hydrophilic part were successfully synthesized and were assembled at Pickering emulsion interfaces,^{29,42-45} however, it is still difficult to control reaction locus on a microscale because it is very challenging to position catalytic sites selectively on one of the parts with nanometer sizes.⁴² In this context, the spatially precisely controlled assembly of catalyst particles at the liquid-liquid interfaces at a microscopic level for selective catalysis remains a persistent, unresolved challenge.

Herein, we demonstrate a novel strategy for regulation of the catalytic selectivity through exquisite control of the liquid-liquid interfacial reaction within Pickering emulsions at a microscopic level. It is exemplified by selective hydrogenation of α,β -unsaturated aldehydes. It was found that the assembly of catalyst particles right at the inner interfacial layer of Pickering emulsion droplets gave 97.6% selectivity to C=O hydrogenation, much higher than those at the outer interfacial layer, within the interior of droplets and at the conventionally-called Pickering emulsion interfaces (which includes both outer and inner layers, namely composite interface). We attempt to clarify the origins for such an unexpected selectivity enhancement effect. Our strategy for the precise control of catalyst assembly at liquid-liquid interfaces and the novel phenomena of interfacial catalysis constitute an important supplement to the existing methods for the tuning catalytic selectivity through regulating the electronic state and structure of catalysts.

2. EXPERIMENTAL SECTION

2.1 Preparation of TNTs-C and TNTs-C⁺. Titanate nanotubes (TNTs) were obtained by an alkaline hydrothermal treatment of TiO₂, as described by Kasuga.⁴⁶ Typically, 3 g anatase was dispersed in NaOH solution (120 mL, 10 mol L⁻¹) and placed in a stainless steel autoclave at 150 °C for 24 h. The precipitate was washed with HCl solution (0.1 M) and deionized water until pH < 8. This was then dried in an air circulating oven at 80 °C for 5 h, thus yielding TNTs. An amount of 1.0 g “as-synthesized” TNTs was dispersed into toluene (6 mL). A mixture of 5 mmol CH₃Si(OCH₃)₃ and 5 mmol (C₂H₅)₃N were added into this toluene suspension. After refluxing at 120 °C for 6 h under a N₂ atmosphere, the obtained material was isolated through centrifugation. The sample was washed five times with toluene and then dried under air. The resultant methyl-functionalized TNTs are denoted as TNTs-C. For TNTs-C⁺, 10 mmol CH₃Si(OCH₃)₃ and 10 mmol (C₂H₅)₃N were used. Other procedures are the same as those for TNTs-C.

2.2 General Procedure for Preparing Pickering Emulsion Reaction Systems. Typically, 2.5 mL deionized water and 2.5 mL toluene were added into a 10 mL vessel containing 0.03 g TPPTS, a certain amount of the emulsifier and the catalyst (if needed). For the inner

interfacial layer reaction, 0.05 g Ru@TNTs as catalyst and 0.05 g TNTs-C as emulsifier; for the droplet interior reaction, 0.05 g Ru@TNTs as catalyst and 0.05 g SiO₂-C as emulsifier; for the composite interfacial reaction, 0.05 g Ru@TNTs-C as both catalyst and emulsifier; for the outer interfacial layer reaction, 0.05 g Ru@TNTs-C⁺ as catalyst (added after forming Pickering emulsion) and 0.05 g TNTs-C as emulsifier. After vigorously stirring (10,000 rpm) with a homogenizer for 2 min, w/o Pickering emulsions were obtained. Then, 1.0 mmol substrate was added for reaction into the continuous oil phase.

2.3 Hydrogenation in w/o Pickering Emulsion Systems. The above Pickering emulsion reaction mixture was loaded in a vessel (10 mL), and the vessel was placed in a 100 mL autoclave. Before the reaction, the autoclave was sealed and flushed with H₂ three times in order to remove any air. Afterwards the autoclave was charged with H₂ at a pressure of 3 MPa at room temperature. The sample was heated to 60 °C within 20 min and was kept at this temperature while being stirred (700 rpm). Following the reaction, the autoclave was cooled to room temperature. The products were isolated through centrifuging and then analyzed by gas chromatography (Agilent 7890A). This was equipped with a HP-5 capillary column. The resulting structures were confirmed by GC-MS (Agilent 7890B GC/5977A MS, HP-5 column). After each run, the organic phase was separated from the reaction system also by centrifuging, where the solid catalyst and emulsifier remained in the aqueous phase. In the next reaction cycle, 2.5 mL of fresh toluene and a given amount of substrate were added into the above system. All the other procedures are the same as those already described for the first reaction.

3. RESULTS AND DISCUSSION

3.1 Preparation and Characterization of Emulsifiers and Catalysts. We chose Pickering emulsions to create the large liquid-liquid interfaces because solid particles assembled at the interfaces lead to more stable emulsion droplets in comparison to surfactant-stabilized emulsions.³⁸ Titanate nanotubes (TNTs) were selected to serve as the emulsifier for preparing Pickering emulsions. Such a choice is based on the following considerations: (i) the narrow width of the nanotubes is helpful for the control of the interfacial reaction occurring in nanoscale regions; (ii) the hollow structure can accommodate catalytic sites, e.g. metal nanoparticles.⁴⁷ After modification with CH₃Si(OCH₃)₃ (silylation of surface Ti-OH), the nanotubes were transformed to an effective particle emulsifier, named as TNTs-C. Fourier transform infrared (FT-IR) spectra (Figure S1) and thermogravimetric (TG) analysis (Figure S2) confirm the successful modification. The loading of methyl groups was determined to be 0.5 mmol g⁻¹ by elemental analysis. As the transmission electron microscopy (TEM) images in Figure 1A and Figure 1B

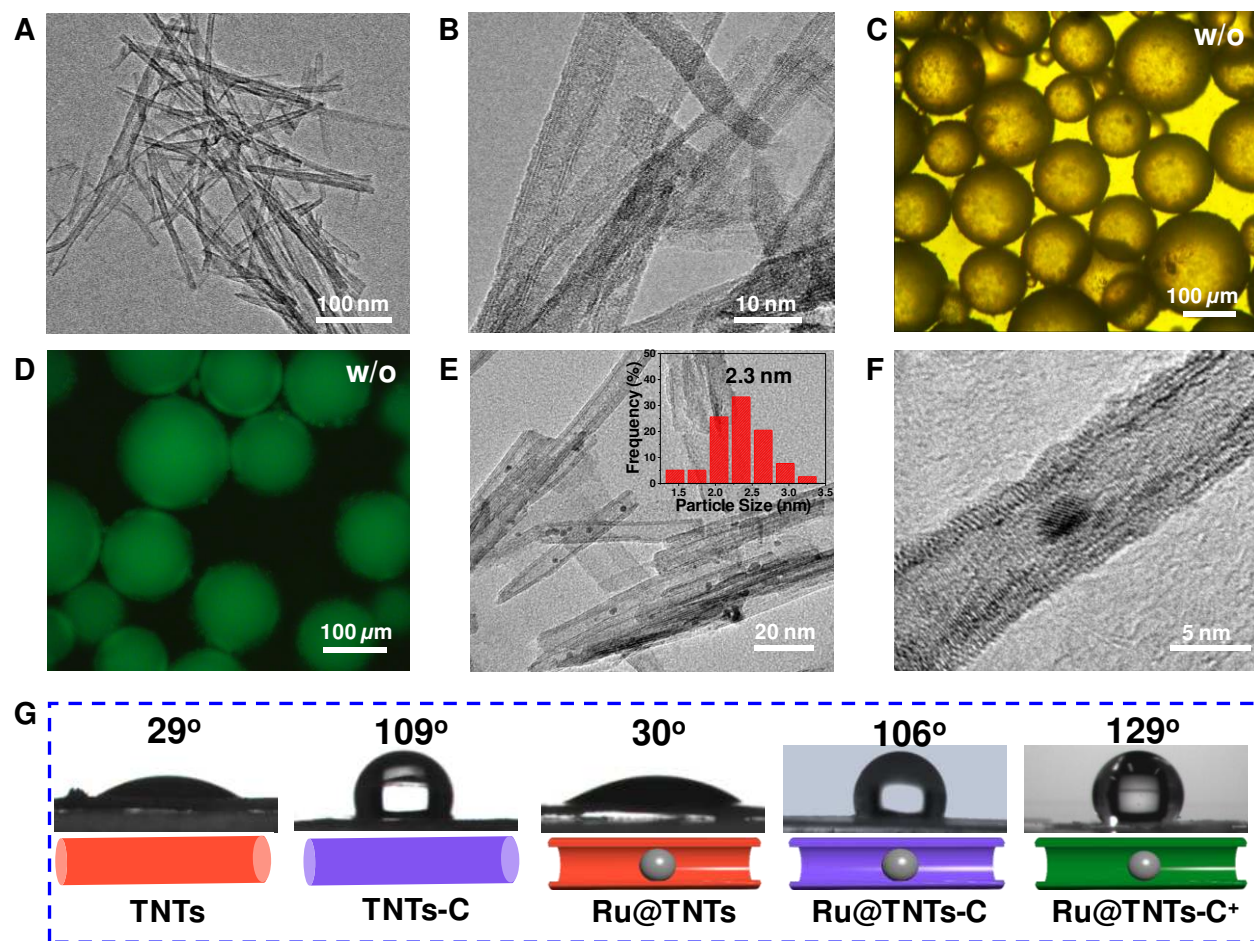


Figure 1. TEM images and water contact angles of different TNTs materials and micrographs of the w/o Pickering emulsion prepared with 2 wt % TNTs-C (with respect to water). (A) TEM image of TNTs. (B) TEM image of TNTs-C. (C) Optical micrograph of the Pickering water-in-toluene emulsion. (D) Fluorescence confocal microscopy image of the Pickering emulsion with the water phase dyed by FITC-I. (E) TEM image of Ru@TNTs, inset showing Ru nanoparticle size distribution. (F) High magnification TEM image of the Ru@TNTs catalyst. (G) Water-air contact angles of various samples.

show, the bare TNTs and TNTs-C are both 100–400 nm in length and 4–7 nm in width, and exhibit a uniform hollow tubular structure open at both ends. The inner pore width is 6.7 nm on average, agreeing with the N_2 sorption analysis results (Figure S3). TNTs before modification are highly hydrophilic per se since the contact angle of a water drop in air is only 29° (Figure 1G), while TNTs-C become partially hydrophobic on account of the methyl groups grafted on their surfaces (exhibiting a water contact angle of 109° , Figure 1G). Using TNTs-C as emulsifier allowed us to formulate water-in-toluene (w/o) Pickering emulsions with droplet sizes of 50–150 μm (Figure 1C), which was further confirmed by fluorescent dyeing of water (Figure 1D). Ru was chosen as a catalytically active metal because it is much less expensive compared to other noble metals. Ru nanoparticles (2–3 nm) were introduced into the interior of TNTs through impregnation of $\text{RuCl}_3 \cdot 3\text{H}_2\text{O}$ followed by reduction (Supporting Experimental Section), leading to a Ru@TNTs catalyst.⁴⁸ This catalyst is highly hydrophilic since its water contact is 30° (Figure 1G). The

TEM images (Figure 1E and Figure 1F) and the X-ray diffraction (XRD) patterns (Figure S4) reveal that Ru nanoparticles were positioned on the inner walls of titanate nanotubes with a high dispersion. Besides the hydrophilic Ru@TNTs catalyst, we also prepared two other hydrophobic catalysts by varying the methyl loading using a similar method: partially hydrophobic catalyst Ru@TNTs-C and more hydrophobic catalyst Ru@TNTs-C⁺. Their water contact angles are 106° and 129° , respectively (Figure 1G).

3.2 Identification of the Liquid-Liquid Interface Impact on Selectivity. Prior to investigating the hydrogenation reactions within Pickering emulsions, we examined the reactions occurring in a single toluene phase, in a single water phase and at a “planar” water-toluene interface (conventional biphasic system), aiming at establishing the impact of the liquid-liquid interface on the reaction outcome (Figure 2A). To obtain good reaction activity and selectivity, tri(sodiumphenylsulfonate)phosphine (TPPTS) was added at a fixed

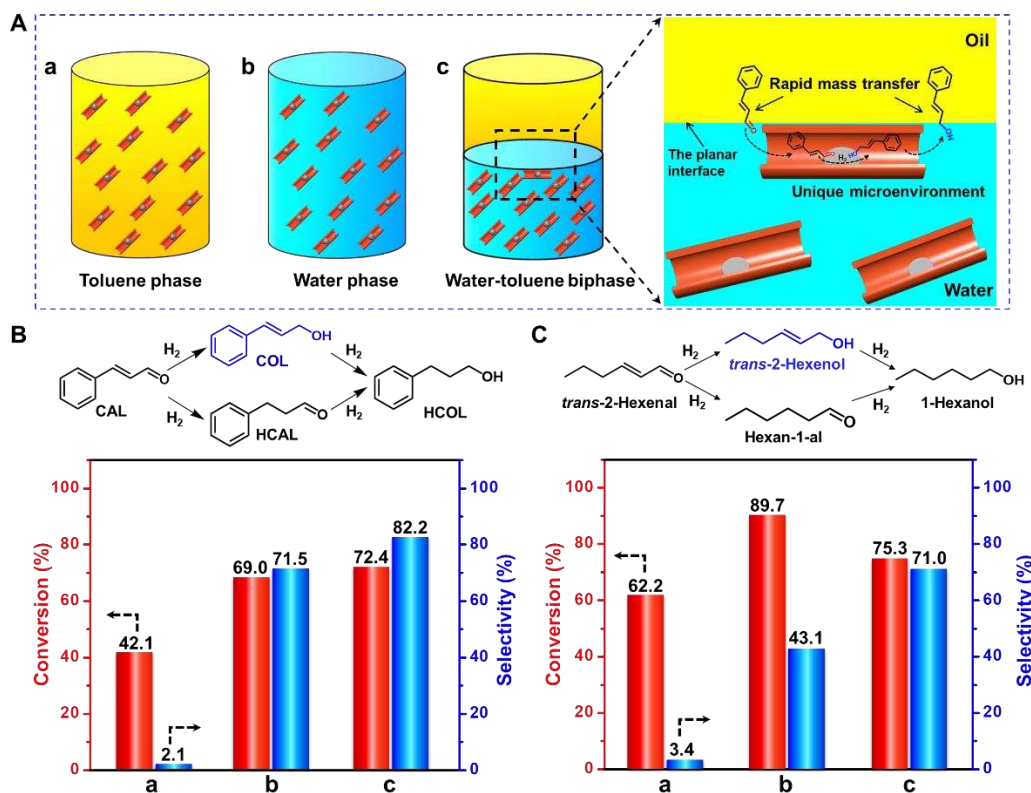


Figure 2. Conversion and selectivity of α,β -unsaturated aldehydes hydrogenation in different reaction systems. (A) Cartoon representing the different reaction systems: (a) single organic phase (5 mL toluene as solvent), (b) single aqueous phase (5 mL water as solvent), (c) water (2.5 mL)-toluene (2.5 mL) biphasic system and corresponding schematic illustration of the reaction taking place at the planar interface (TPPTS is omitted for clarification). Conversion and selectivity of (B) CAL and (C) *trans*-2-hexenal in different reaction systems. Reaction conditions: 0.05 g Ru@TNTs, 0.03 g TPPTS, 1.0 mmol CAL or *trans*-2-hexenal, 3.0 MPa H₂, 60 °C, 700 rpm, 5 h.

concentration into the reaction systems catalyst for cinnamaldehyde (CAL) hydrogenation since the CAL conversion and the selectivity to cinnamyl (Figure S5). One of the roles of TPPTS is to server as water-soluble ligand modifying the Ru nanoparticle surface to improve the conversion and selectivity. Such a surface modification was confirmed by X-ray photoelectron spectroscopy in Figure S6 and solid-state ³¹P MAS NMR spectra in Figure S7. Ru@TNTs with the aid of TPPTS proved a good alcohol (COL, desired product) is much better than a Ru/SiO₂ catalyst or a Ru/TiO₂ catalyst (using commercial TiO₂ particles as support, Figure S5). It was notable that the methyl modification of the TNTs itself had a negligible effect on the catalytic performance since Ru@TNTs, Ru@TNTs-C and Ru@TNTs-C⁺ are completely comparable in terms of selectivity and activity in a water-ethanol system (Table S1). Under the same conditions, the single toluene system gave 42.1% conversion of CAL and 2.1% selectivity to COL, whereas the conversion and selectivity in the single water system were dramatically increased up to 69.0% and 71.5%, respectively (Figure 2B). Interestingly, in the water-toluene biphasic system, the conversion and selectivity were improved up to 72.4% and 82.2%. For another

substrate *trans*-2-hexenal, these three systems also exhibited very different reaction outcomes (Figure 2C). The selectivity to C=O obtained in the biphasic system was much higher than that obtained in the single water phase or single toluene phase. Moreover, this hydrogenation in the biphasic system gave much higher selectivity than those in other common organic solvents (Table S2). These results highlight an oil-water interfacial effect that impacts the catalytic selectivity. It was previously found that “on water” effects⁴⁹⁻⁵¹ and H-shuttle effects caused by the presence of water were reported to improve the reaction rate or alter the reaction selectivity.⁵²⁻⁵⁶ However, in our case, the selectivity enhancement should not be attributed to the effects arising from the presence of water molecules since the oil-water biphasic system gave much higher selectivity than the single water system (82.2% vs 71.5%). The presence of a liquid-liquid interface (biphasic system) should be responsible for the catalytic selectivity enhancement (Figure 2A, c).

3.3 Control of Reaction Locus at Pickering Emulsion Interfaces. Encouraged by the impact of the planar liquid-liquid interface on the selectivity, we

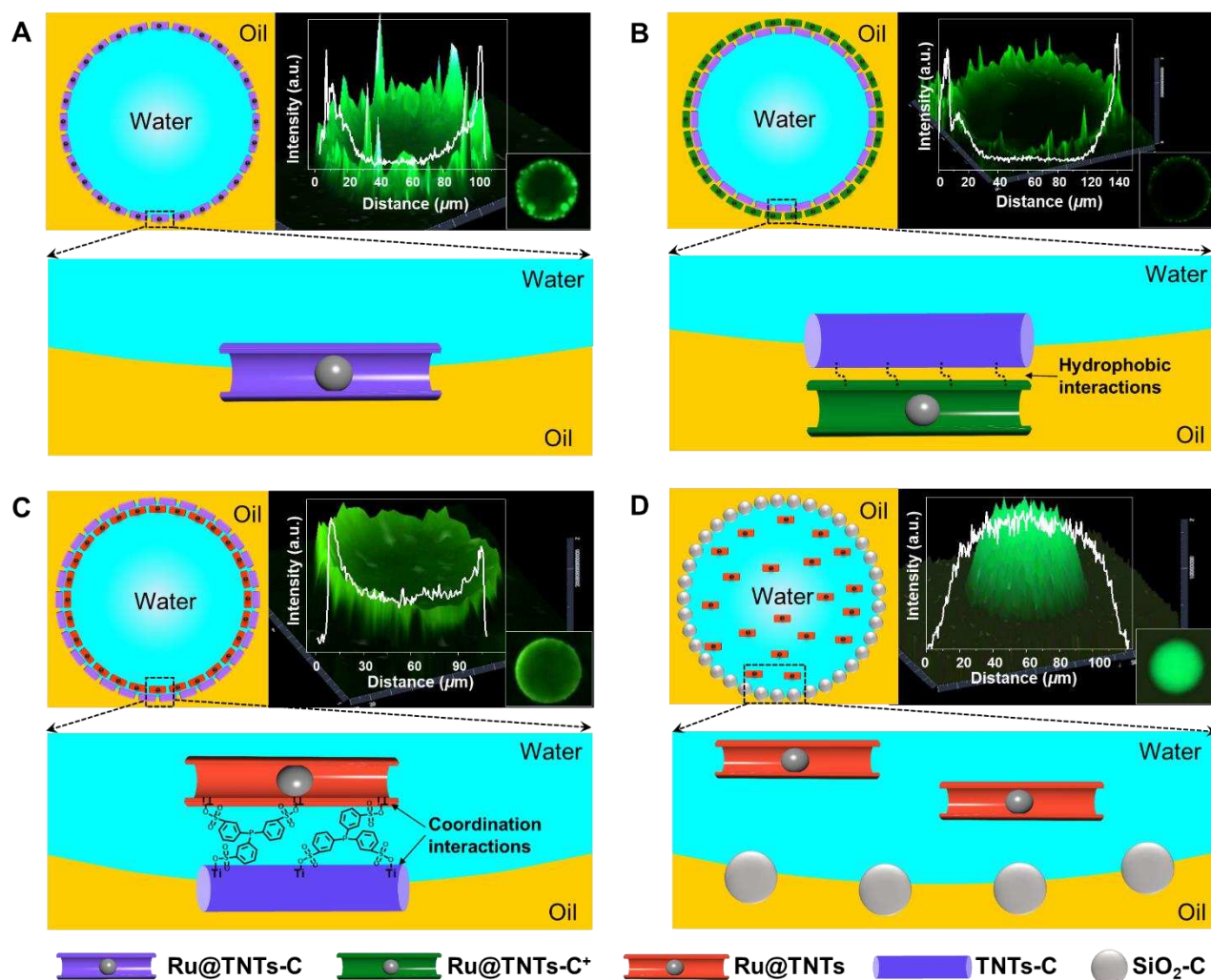


Figure 3. Cartoon describing the catalyst locations within w/o Pickering emulsions and corresponding 3D fluorescence confocal micrographs. (A) Catalyst is located at the conventionally-called Pickering emulsion interface. (B) Catalyst is located at the outer interfacial layer of water droplets. (C) Catalyst is located at the inner interfacial layer of water droplets by the interaction of Ru@TNTs with TNTs-C. (D) Catalyst is distributed in the interior of droplets. The emulsion consists of 2.5 mL toluene, 2.5 mL water, 0.05 g FITC-I-labelled Ru@TNTs-C (for A), 0.05 g FITC-I-labelled Ru@TNTs-C⁺ (for B), 0.05 g FITC-I-labelled Ru@TNTs (for C and D), 0.05 g TNTs-C (for B and C), 0.05 g SiO₂-C (for D), 0.03 g TPPTS. Drawing are not to scale.

transformed the above biphasic system to a Pickering emulsion system, in order to significantly increase the reaction interfacial area through generating numerous droplets (Figure 3). Pickering emulsion reaction systems (w/o) were achieved using shear in the presence of Ru@TNTs-C as both emulsifier and catalyst. The assembly of Ru@TNTs-C particles at water droplet interfaces was evidenced by a fluorescent circle in 3D confocal fluorescence microscopy with FITC-I-labelled Ru@TNTs-C (Figure 3A). For this Pickering emulsion system, the conversion (87.6%) is higher than that obtained in the biphasic system, but the selectivity decreases down to 69.6% (Figure 4A, a). The improved conversion is due to the location of the Ru@TNTs-C

catalyst particles at droplet interfaces, which promotes sufficient contact of the reactant with the catalyst. Such remarkable differences in selectivity caused by the catalyst location prompts us to further consider the interfacial reaction locus at a more microscopic level. In the Pickering emulsion system, the tubular emulsifier particles adopt an orientation parallel to the interface (Figure S8);^{57,58} one side of Ru@TNTs-C protrudes into the water droplet and the other side into the oil phase. These two sides, in fact, make different contributions to the observed reaction outcome because the single aqueous system and the single oil system are very different in selectivity, as revealed above. The spatially

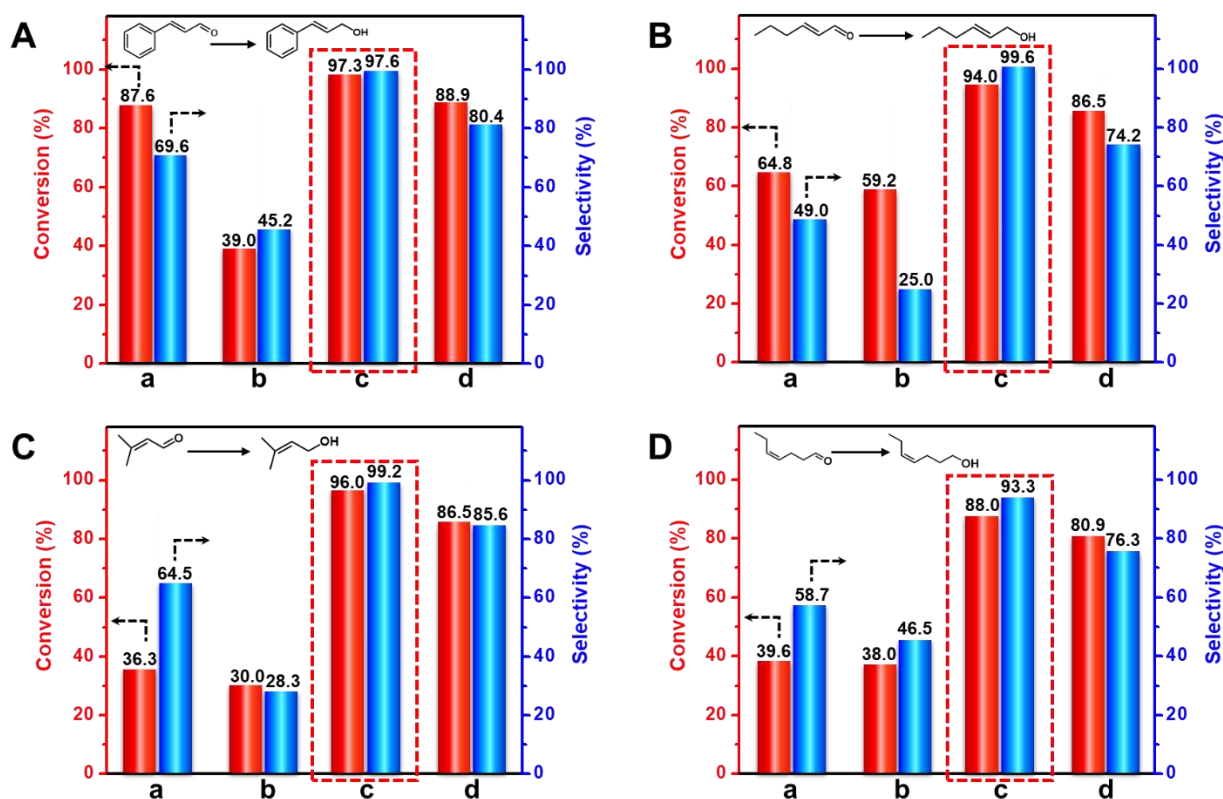


Figure 4. Results of unsaturated aldehydes hydrogenation in different reaction loci within w/o Pickering emulsions: (a) catalyst is located at the conventionally-called Pickering emulsion interface, (b) catalyst is located at the outer interfacial layer of water droplets, (c) catalyst is located at the inner interfacial layer of water droplets, (d) catalyst is distributed in the interior of droplets. Conversion and selectivity for (A) CAL, (B) *trans*-2-hexenal, (C) 3-methyl-2-butenal, and (D) *cis*-4-heptenal hydrogenation in different reaction loci. Reaction conditions: 1.0 mmol unsaturated aldehydes, 2.5 mL toluene, 2.5 mL water, 0.05 g Ru@TNTs-C (for a), 0.05 g Ru@TNTs-C⁺ (for b), 0.05 g Ru@TNTs (for c and d), 0.05 g TNTs-C (for b and c), 0.05 g SiO₂-C (for d), 0.03 g TPPTS, 60 °C, 3.0 MPa H₂, 700 rpm, 5 h.

precise control of the interfacial reaction locus on a microscale and thereby discriminating the composite interfacial reaction (conventionally-called Pickering emulsion interface), the outer interfacial layer reaction, the inner interfacial layer reaction and the reaction within droplet interiors, is necessary and significant.

Fortunately, we unexpectedly found that the unique interaction between TNTs and TPPTS makes possible the spatially controlled assembly of TNTs at the droplet interface (Figure S9). This interaction (to be discussed later) is another role of TPPTS besides the modification of Ru nanoparticles. The use of TNTs-C as emulsifier and Ru@TNTs-C⁺ as catalyst enabled us to position Ru@TNT-C⁺ exclusively at the outer interfacial layer. The location of FITC-I-labelled Ru@TNT-C⁺ at the outer interfacial layer of water droplets was confirmed by the presence of a fluorescent circle whose intensity gradually increases on approaching the interface from outside (Figure 3B). This is because the Ru@TNTs-C⁺ particles *per se* are too hydrophobic to assemble at droplet interfaces (Figure S10a), being initially distributed in the oil phase, and then

spontaneously migrate to the droplet interface due to the weak interactions with the TNTs-C emulsifier in low dielectric toluene (hydrophobic interactions of particles with high aspect ratio^{57,58}), as shown in Figure S11. Conversely, when the Ru@TNTs-C⁺ catalyst was replaced with the hydrophilic Ru@TNTs catalyst (FITC-I-labelled), the catalyst assembled at the inner interfacial layer of water droplets since the intensity of the observed fluorescent circle in Figure 3C decreases from the interface to the droplet center (The Ru@TNTs particles *per se* are too hydrophilic to assemble at droplet interfaces as revealed in Figure S10b; the migration of Ru@TNTs to the inner interface of water droplets was monitored by fluorescence microscopy as shown in Figure S12. The stirring did not cause the change of the location of Ru@TNTs at the inner interfaces due to the strong interactions between Ru@TNTs and TNTs-C through TPPTS bridging effect discussed later, as shown in Figure S13). Moreover, we had attempted to use cryo-TEM to directly observe the location of Ru@TNTs

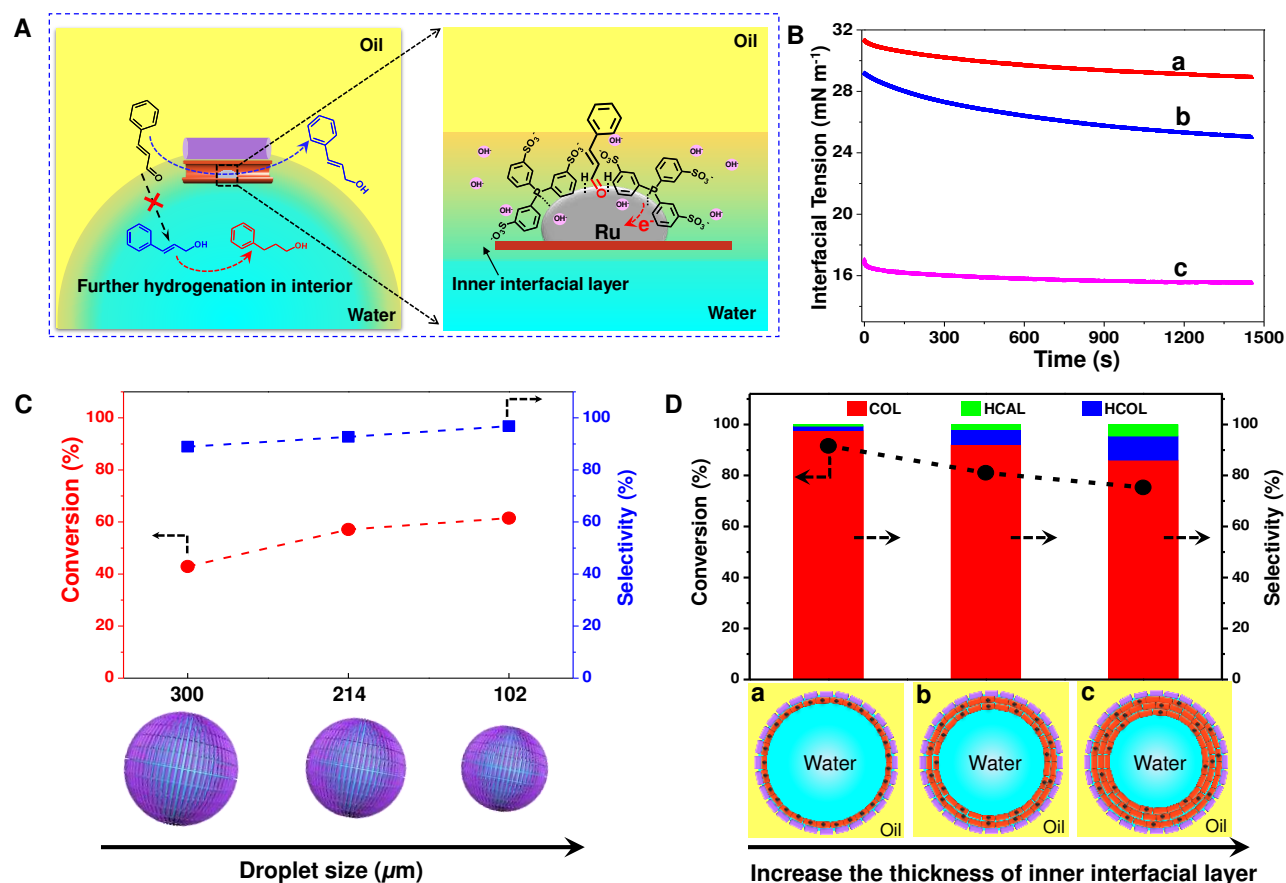


Figure 5. Proposed mechanism and evidence. (A) Schematic illustration of the inner interfacial layer reaction scenario. (B) Dynamic interfacial tensions in different water-toluene biphasic systems: (a) 3 mg mL⁻¹ TPPTS in water, (b) 3 mg mL⁻¹ TPPTS in water and 5 mg mL⁻¹ TNTs-C in toluene, (c) 3 mg mL⁻¹ TPPTS and 5 mg mL⁻¹ TNTs in water, 5 mg mL⁻¹ TNTs-C in toluene. (C) CAL conversion and COL selectivity versus droplet size in the inner interfacial layer reaction system, reaction time: 3 h. (D) CAL conversion and COL selectivity versus the thickness of inner interfacial layer in the inner interfacial layer reaction systems: (a) absence of TNTs, (b) adding 0.025 g TNTs, (c) adding 0.05 g TNTs. Other reaction conditions are same as those in Figure 4.

catalyst. As shown in Figure S14, a few layers of TNTs-C as emulsifiers lie flat at the oil-water interface where no Ru nanoparticles were discerned. Notably, at the inner surface of emulsion droplet the Ru@TNTs catalysts are observed since Ru nanoparticles are present. Finally, when using partially hydrophobic silica particles SiO₂-C as emulsifier (Supporting Experimental Section), the Ru@TNTs particles (FITC-I-labelled) were distributed throughout the interior of the water droplets due to the absence of interactions with the emulsifier at the interfaces, confirmed by a convex fluorescence image (Figure 3D).

Impressively, these different scenarios led to substantial differences in reaction outcome. In the CAL hydrogenation, the outer interfacial layer reaction gave 39.0% conversion and 45.2% selectivity to COL (Figure 4A, b), both much lower than those obtained in the case of the composite interfacial reaction (Figure 4A, a). Such

low conversion and selectivity are due to the difficulty for catalyst particles at the outer interfacial layer to access water-soluble TPPTS. To our delight, the inner interfacial layer reaction gave 97.3% conversion and 97.6% selectivity (Figure 4A, c; other two surface-active additives were also checked, but their results are inferior to those obtained with TPPTS in Table S3). Such a high selectivity outperforms that obtained in most reported catalysts, even including expensive Pt catalysts (Table S4). However, when the reaction occurred within the droplet interior (Figure 4A, d), the CAL conversion and COL selectivity sharply dropped to 88.9% and 80.4%, respectively. For this case, the decrease in conversion can be explained by the fact that the distribution of catalyst within droplet interiors decreases the accessibility to the oil-soluble CAL in comparison to the inner interfacial layer reaction. The lowered selectivity results from the further hydrogenation due partially to the untimely

transfer of COL outside the droplets. The data in Table S5 are in support of this inference since COL was further hydrogenated to hydrocinnamyl alcohol (HCOL, 16.1%) in this case, while only 1.8% HCOL was observed in the inner interfacial layer reaction system. This inference is further supported by the experiment in which the selectivity declined on prolonging the reaction time (Figure S15). Moreover, the remarkable enhancements of reaction efficiency and selectivity for the inner interfacial reaction have been observed in the selective hydrogenation of other unsaturated aldehydes, for example *trans*-2-hexenal, 3-methyl-2-butenal and *cis*-4-heptenal (Figure 4B, Figure 4C and Figure 4D). For all these investigated substrates, the selectivity to C=O hydrogenation is as high as 93.3–99.6%. Such an excellent selectivity is not easily obtained for the reported single phase systems.^{4,10} Based on these results, we can conclude that the difference in selectivity is caused by changes in the reaction locus, and the assembly of catalyst particles exclusively at the inner interfacial layer significantly boosts the selectivity (the possibility of the influence of droplet surface coverage is excluded, as displayed in Figure S16).

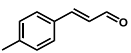
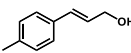
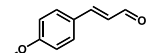
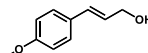
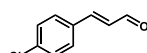
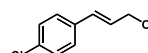
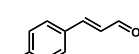
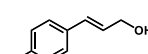
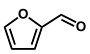
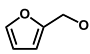
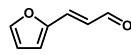
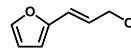
3.4 Reasons for Selectivity Enhancement. With such interesting results, we become aware of the unique mechanism of the formation of the inner interfacial layer for highly selective catalysis (Figure 5A). The process of the assembly of Ru@TNTs at the inner interfacial layer was tracked by fluorescence labelling (Figure S12). The FITC-I-labelled Ru@TNTs were dispersed in water, and the TNTs-C emulsifier particles were dispersed in toluene. Immediately after emulsification of a mixture of these two suspensions, the fluorescence intensity at the inner droplet interface gradually increased and then levelled off, while the fluorescence intensity of the interior of a droplet gradually decreased and levelled off after 10 min. This indicates that Ru@TNTs migrated from the interior of a droplet to the inner interface. The driving force for such an assembly was found to be related to the presence of TPPTS since the migration of Ru@TNTs towards the interface was not observed when TPPTS was absent (Figure S9). The FT-IR spectrum results reveal that TPPTS tends to adsorb onto TNTs because the $-\text{SO}_3^-$ groups in TPPTS are coordinated with surface 4-coordinated Ti (Figure S17; Despite the methyl modification, the surface coordination interactions between uncovered Ti sites and $-\text{SO}_3^-$ groups still exists).⁵⁹ Owing to the interactions, TPPTS bearing three $-\text{SO}_3^-$ groups can bridge the TNTs-C emulsifier and the Ru@TNTs catalyst (Figure 3C, the other role of TPPTS), thus forming an inner interfacial layer. This inference is also supported by the following experiments. Ligands containing two $-\text{SO}_3^-$ groups, such as disodium

piperazine-1,4-diethanesulphonate and disodium butane-1,4-disulfonate, exhibited an effect similar to TPPTS but sodium allylsulfonate and sodium benzenesulfonate containing only one sulfonate group did not (Figure S18). These experiments confirm that the additive containing two or more $-\text{SO}_3^-$ groups is necessary for the assembly of catalyst particles at the inner interfacial layer.

Dynamic interfacial tension measurements further support the interactions between Ru@TNTs and TNTs-C in the presence of TPPTS (Figure 5B). The equilibrium toluene-water interfacial tension in the presence of TPPTS was measured to be 28.9 mN m⁻¹. The interfacial tension decreased to 25.0 mN m⁻¹ after adding TNTs-C particles, due to the adsorption of nanoparticles.⁵⁷ Notably, when TNTs particles were introduced into the above system, the interfacial tension further declined to 15.5 mN m⁻¹, reflecting the adsorption of TNTs onto the interface due to the interaction with the TNTs-C. In contrast, if TNTs-C particles are replaced with the interface-active SiO₂-C particles, the interfacial tension does not significantly decrease after adding TNTs (23.8 mN m⁻¹, Figure S19), indicating the migration of TNTs to the interface did not occur (the SiO₂-C surface lacks the coordination interaction with TPPTS). These findings are consistent with the aforementioned fluorescence observations.

Based on the supportive results, we propose a mechanism for the inner interfacial reaction with high selectivity. Prior to the investigation of the interface role, we compared the Ru@TNTs catalyst with the Ru/TNTs catalyst on which Ru nanoparticles are located on outside of the titanate nanotube (Figure S20). The comparative results reveal that the different Ru nanoparticle location had similar reaction outcome, ruling out the possibility of the impact of the nanotube confinement space on the selectivity. As Figure 5A illustrates, the oil-soluble CAL can relatively easily contact the catalyst assembled at the inner interfacial layer, where TPPTS is enriched (supported by the results of interfacial tension in Figure 5B).^{61,62} The TPPTS enriched at the droplet interfaces leads to the high selectivity, which is supported by the finding that the selectivity is gradually increased upon increasing the TPPTS concentration in a water-toluene biphasic system (Figure S21). Additionally, the high selectivity is also related to the timely and instant removal of COL from the inner interfacial layer to the outside of droplets, due to the shorter diffusion distance compared to the case where the reaction occurs in the droplet interior. Further hydrogenation of the C=C bond was accordingly avoided. This agrees with the findings that the COL selectivity decreased as reaction time was prolonged in both an aqueous system and a water-

Table 1. Selective hydrogenation of different unsaturated aldehydes within different w/o Pickering emulsion systems.^a

Entry	Reactant	Product	Conv. (%)	Sel. (%)
1 ^b			97.0 (63.0)	91.6 (84.6)
2 ^b			99.0 (59.0)	95.4 (73.0)
3			99.3 (46.5)	95.0 (89.2)
4			96.4 (60.5)	97.5 (79.6)
5			97.0 (60.2)	98.3 (87.1)
6			92.4 (56.0)	95.0 (88.5)

^aNumbers in brackets refer to the results obtained in the composite interface reaction within the conventional Pickering emulsions. Reaction conditions: 1.0 mmol unsaturated aldehydes, 2.5 mL toluene, 2.5 mL water, 0.05 g catalyst, 0.05 g emulsifier, 0.03 g TPPTS, 60 °C, 3.0 MPa H₂, 700 rpm, 4 h. ^b4.0 MPa H₂, 6 h.

toluene biphasic system, while the HCOL selectivity increased upon prolonging the reaction time (Figure S15). The resultant unique local microenvironment led to high catalytic activity. Moreover, the basicity of water droplet interfaces (due to enriching of OH⁻) that was reported in literature,^{63,64} may also play a certain part in improving the selectivity since the CAL hydrogenation carried out at different pH values showed that the COL selectivity increased from 71.5% to 81.8% when the pH increased from 7 to 11 in a single water system (Figure S22), which is consistent with the reported results.⁴ Taken together, although the liquid-liquid interface effect is relatively complicated, involving multiple factors such as ligand enriching effects, mass transport, basicity, and harnessing of these features can really improve the catalytic selectivity as revealed here. To further confirm this interface effect, we also replaced TPPTS with disodium butane-1,4-disulfonate that can bridge TNTs-C and Ru@TNTs but cannot modify Ru nanoparticles because of the absence of phosphine ligand. It was found that the COL selectivity was also improved at the inner interfacial layer in comparison to the case of droplet interior reaction where disodium butane-1,4-disulfonate

was not added (notably, disodium butane-1,4-disulfonate itself has no effect on the selectivity and CAL conversion, as revealed by Table S6).

To further investigate the effects stemming from the inner interfacial layer, we studied the influence of average droplet size, thickness of inner interfacial layer as well as TPPTS dosage. The reaction systems with different droplet sizes were achieved by varying the stirring rate during emulsification. Upon decreasing the droplet diameter from 300 μm to 214 μm and further to 102 μm (Figure S23), the CAL conversion increased gradually from 42.9% to 57.1% and then to 61.5%, and the COL selectivity increased from 88.9% to 92.7% and then to 96.8% (Figure 5C). These increases in conversion and selectivity are caused by the increase in the total area of inner interface that manifests the inner interfacial effects. Moreover, by adding different amounts of catalytically inactive TNTs together with a fixed amount of the Ru@TNTs catalyst, we could change the thickness of the inner interfacial layer, as depicted in Figure 5D. It was found that the CAL conversion and COL selectivity both decreased with increasing the thickness of the inner interfacial layer. This finding suggests that narrowing of the inner interfacial layer is crucial to obtaining high selectivity and conversion. This is probably because the narrow inner interfaces facilitate the rapid mass transfer of COL from the inner interfacial layer to the outside of droplets, and the further hydrogenation is avoided. Additionally, we compared the inner interfacial reaction with the conventional biphasic reaction in terms of dosage of TPPTS. There is only a small decrease in selectivity (from 97.6% to 94.0%) upon decreasing the dosage of TPPTS for the inner interfacial reaction (Figure S24), whereas a substantial decrease in COL selectivity was observed in the conventional biphasic system (from 82.2% to 65.3%). The negligibly small decrease in COL selectivity is attributed to the inner interfacial effect that is in favor of enriching TPPTS. The findings from these three aspects further highlight the uniqueness and importance of the inner interfacial reaction.

3.5 Substrate Scope and Recyclability. The substrate scope was further extended to other unsaturated aldehydes beyond those in Figure 4. As summarized in Table 1, for all the investigated substrates including various phenyl and furyl-containing unsaturated aldehydes, the inner interfacial layer reaction gave conversion of 92.4–99.3% and selectivity of 91.6–98.3%, which are all higher than those obtained in the composite interfaces of Pickering emulsions (data in parentheses as benchmark). These results further confirm that our liquid-liquid interface strategy is generally more effective at improving the catalytic selectivity.

Another advantage of our system is the good recyclability of the catalyst (Figure S25). After the first run, the Pickering emulsion was demulsified *via* centrifugation. The upper layer of toluene containing product was collected by liquid transfer, and the lower aqueous layer containing catalysts and TPPTS was used directly for the second reaction cycle. After adding fresh reactant and toluene followed by emulsification, a w/o Pickering emulsion reaction system was obtained again. In the fourth reaction cycle, the conversion and selectivity reached 91.3% and 91.8%, respectively (Figure S25a). This slight decrease was caused by the loss of emulsifier and catalyst during multiple cycles. After four reaction cycles, the Ru content on the catalyst decreased from 1.6 wt.% to 1.24 wt.% according to the ICP results. The micro-structure of catalyst particles did not change significantly, as revealed by TEM images (Figure S26). The loss of emulsifier led to an increase in droplet size, weakening inner interface effects (Figure S25b).

4. CONCLUSION

We have successfully demonstrated a strategy of liquid-liquid interface to improve catalytic selectivity. The key to this success is the precise assembly of tubular catalyst particles at the inner interface of w/o Pickering emulsion droplets. It is found that for all investigated α,β -unsaturated aldehydes the selectivity and catalysis efficiency for the inner interfacial layer reaction are much higher than those obtained for all of the composite interface reaction within Pickering emulsions, the outer interfacial layer reaction within Pickering emulsions, the reaction within droplet interiors and reactions in single aqueous or organic phases. 92.0–98.0% selectivity to the thermodynamically and kinetically unfavorable C=O hydrogenation over C=C hydrogenation was achieved unexpectedly. The significant enhancement in catalytic selectivity is attributed to the unique microenvironment of the inner interfacial layer of water droplets and the timely departure of unsaturated alcohol from the water droplet avoiding further hydrogenation. We envisage that the strategy of spatially precisely controlled assembly of catalysts in liquid-liquid interfaces together with the observed phenomenon of selectivity enhancement at the interfaces opens a new way to tune catalytic selectivity.

ASSOCIATED CONTENT

Supporting Information

Synthesis and characterization details, the results of hydrogenation of unsaturated aldehydes in different conditions, MS data for products. This material is available free of charge via the Internet at <http://pubs.acs.org>.

AUTHOR INFORMATION

Corresponding Author

Hengquan Yang—School of Chemistry and Chemical Engineering, Shanxi University, Taiyuan 030006, China; Email: hqyang@sxu.edu.cn

Authors

Yabin Zhang—School of Chemistry and Chemical Engineering, Shanxi University, Taiyuan 030006, China

Rammile Ettelaie—Food Colloids Group, School of Food Science and Nutrition, University of Leeds, Leeds LS2 9JT, U.K.

Bernard P. Binks—Department of Chemistry and Biochemistry, University of Hull, Hull. HU6 7RX. U.K.

Notes

The authors declare no competing financial interests.

ACKNOWLEDGMENT

This work was supported by the Natural Science Foundation of China (21733009, 21925203). BPB acknowledges funding from the H2020-FETOPEN-2016-2017 program of the European Commission (grant agreement no. 737266-ONE FLOW).

REFERENCES

- (1) Schlögl, R. Heterogeneous Catalysis. *Angew. Chem. Int. Ed.* **2015**, *54*, 3465–3520.
- (2) Zheng, R. Y.; Liu, Z. C.; Wang, Y. D.; Xie, Z. K. Industrial Catalysis: Strategies to Enhance Selectivity. *Chin. J. Catal.* **2020**, *41*, 1032–1038.
- (3) Tamura, M.; Yonezawa, D.; Oshino, T.; Nakagawa, Y.; Tomishige, K. In Situ Formed Fe Cation Modified Ir/MgO Catalyst for Selective Hydrogenation of Unsaturated Carbonyl Compounds. *ACS Catal.* **2016**, *7*, 5103–5111.
- (4) Lan, X. C.; Wang, T. F. Highly Selective Catalysts for the Hydrogenation of Unsaturated Aldehydes: A Review. *ACS Catal.* **2020**, *10*, 2764–2790.
- (5) Wu, B. H.; Huang, H. Q.; Yang, J.; Zheng, N. F.; Fu, G. Selective Hydrogenation of α,β -Unsaturated Aldehydes Catalyzed by Amine-Capped Platinum-Cobalt Nanocrystals. *Angew. Chem. Int. Ed.* **2012**, *51*, 3440–3443.
- (6) Schoenbaum, C. A.; Schwartz, D. K.; Medlin, J. W. Controlling the Surface Environment of Heterogeneous Catalysts Using Self-Assembled Monolayers. *Acc. Chem. Res.* **2014**, *47*, 1438–1445.
- (7) Cano, I.; Chapman, A. M.; Urakawa, A.; van Leeuwen, P. W. N. M. Air-Stable Gold Nanoparticles Ligated by Secondary Phosphine Oxides for the Chemoselective Hydrogenation of Aldehydes: Crucial Role of the Ligand. *J. Am. Chem. Soc.* **2014**, *136*, 2520–2528.
- (8) Ouyang, R.; Jiang, D. E. Understanding Selective Hydrogenation of α,β -Unsaturated Ketones to Unsaturated Alcohols on the Au₂₅(SR)₁₈ Cluster. *ACS Catal.* **2015**, *5*, 6624–6629.
- (9) Bai, S. X.; Bu, L. Z.; Shao, Q.; Zhu, X.; Huang, X. Q. Multicomponent Pt-Based Zigzag Nanowires as Selectivity

Controllers for Selective Hydrogenation Reactions. *J. Am. Chem. Soc.* **2018**, *140*, 8384–8387.

(10) Zhao, M. T.; Yuan, K.; Wang, Y.; Li, G. D.; Guo, J.; Gu, L.; Hu, W. P.; Zhao, H. J.; Tang, Z. Y. Metal–Organic Frameworks as Selectivity Regulators for Hydrogenation Reactions. *Nature* **2016**, *539*, 76–80.

(11) Mitsudome, T.; Matoba, M.; Yamamoto, M.; Mizugaki, T.; Jitsukawa, K.; Kaneda, K. Remarkable Effect of Bases on Core-Shell AgNP@CeO₂ Nanocomposite-catalyzed Highly Chemoselective Reduction of Unsaturated Aldehydes. *Chem. Lett.* **2013**, *42*, 660–662.

(12) Wu, Q. F.; Zhang, C.; Arai, M.; Zhang, B.; Shi, R. H.; Wu, P. X.; Wang, Z. Q.; Liu, Q.; Liu, K.; Lin, W. W.; Cheng, H. Y.; Zhao, F. Y. A Pt/TiH₂ Catalyst for Ionic Hydrogenation via Stored Hydrides in the Presence of Gaseous H₂. *ACS Catal.* **2019**, *9*, 6425–6434.

(13) Wang, X. F.; Liang, X. H.; Geng, P.; Li, Q. B. Recent Advances in Selective Hydrogenation of Cinnamaldehyde over Supported Metal-Based Catalysts. *ACS Catal.* **2020**, *10*, 2395–2412.

(14) Liu, H. L.; Yuan, M. L.; Guo, C. H.; Li, R. X.; Fu, H. Y.; Chen, H.; Li, X. J. Selective Hydrogenation of Cinnamaldehyde to Cinnamyl Alcohol over Ru/ZrO₂·xH₂O Catalyst. *Chin. J. Catal.* **2011**, *32*, 1256–1261.

(15) Tamura, M.; Yonezawa, D.; Oshino, T.; Nakagawa, Y.; Tomishige, K. In Situ Formed Fe Cation Modified Ir/MgO Catalyst for Selective Hydrogenation of Unsaturated Carbonyl Compounds. *ACS Catal.* **2017**, *7*, 5103–5111.

(16) Martínez-Prieto, L. M.; Puche, M.; Cerezo-Navarrete, C.; Chaudret, B. Uniform Ru Nanoparticles on N-doped Graphene for Selective Hydrogenation of Fatty Acids to Alcohols. *J. Catal.* **2019**, *377*, 429–437.

(17) Dai, Y. H.; Chu, X. F.; Gu, J. J.; Gao, X.; Xu, M.; Lu, D.; Wan, X. Y.; Qi, W.; Zhang, B. S.; Yang, Y. H. Water-Enhanced Selective Hydrogenation of Cinnamaldehyde to Cinnamyl Alcohol on RuSnB/CeO₂ Catalysts. *Appl. Catal. A: Gen.* **2019**, *582*, 117098.

(18) Yang, Y. S.; Rao, D. M.; Chen, Y. D.; Dong, S. Y.; Wang, B.; Zhang, X.; Wei, M. Selective Hydrogenation of Cinnamaldehyde over Co-Based Intermetallic Compounds Derived from Layered Double Hydroxides. *ACS Catal.* **2018**, *8*, 11749–11760.

(19) Chatterjee, M.; Ikushima, Y.; Zhao, F. Y. Completely Selective Hydrogenation of *trans*-Cinnamaldehyde to Cinnamyl Alcohol Promoted by a Ru–Pt Bimetallic Catalyst Supported on MCM-48 in Supercritical Carbon Dioxide. *New J. Chem.* **2002**, *27*, 510–513.

(20) Fujita, S. I.; Sano, Y.; Bhanage, B. M.; Arai, M. Supported Liquid-phase Catalysts Containing Ruthenium Complexes for Selective Hydrogenation of α,β -unsaturated Aldehyde: Importance of Interfaces Between Liquid Film, Solvent, and Support for the Control of Product Selectivity. *J. Catal.* **2004**, *225*, 95–104.

(21) Piradashvili, K.; Alexandrino, E. M.; Wurm, F. R.; Landfester, K. Reactions and Polymerizations at the Liquid-Liquid Interface. *Chem. Rev.* **2016**, *116*, 2141–2169.

(22) Benjamin, I. Reaction Dynamics at Liquid Interfaces. *Annu. Rev. Phys. Chem.* **2015**, *66*, 165–188.

(23) Agmon, N.; Bakker, H. J.; Campen, R. K.; Henschman, R. H.; Pohl, P.; Roke, S.; Thamer, M.; Hassanali, A. Protons and Hydroxide Ions in Aqueous Systems. *Chem. Rev.* **2016**, *116*, 7642–7672.

(24) Zhao, G. L.; Li, Y.; Hong, B.; Han, X.; Zhao, S. L.; Pera-Titus, M.; Liu, H. L. Nanomixing Effects in Glycerol/Dodecanol

Pickering Emulsions for Interfacial Catalysis. *Langmuir* **2018**, *34*, 15587–15592.

(25) Bain, R. M.; Pulliam, C. J.; Thery, F.; Cooks, R. G. Accelerated Chemical Reactions and Organic Synthesis in Leidenfrost Droplets. *Angew. Chem. Int. Ed.* **2016**, *55*, 10478–10482.

(26) Dong, N.; Zhang, Z. P.; Xue, X. S.; Li, X.; Cheng, J. P. Phosphoric Acid Catalyzed Asymmetric 1,6-Conjugate Addition of Thioacetic Acid to para-Quinone Methides. *Angew. Chem. Int. Ed.* **2016**, *55*, 1460–1464.

(27) Zhang, B. Y.; Jiang, Z. X.; Zhou, X.; Lu, S. M.; Li, J.; Liu, Y.; Li, C. The Synthesis of Chiral Isotetronic Acids with Amphiphilic Imidazole/Pyrrrolidine Catalysts Assembled in Oil-in-Water Emulsion Droplets. *Angew. Chem. Int. Ed.* **2012**, *51*, 13159–13162.

(28) Hayashi, Y.; Aratake, S.; Okano, T.; Takahashi, J.; Sumiya, T.; Shoji, M.; Combined Proline–Surfactant Organocatalyst for the Highly Diastereo- and Enantioselective Aqueous Direct Cross-Aldol Reaction of Aldehydes. *Angew. Chem. Int. Ed.* **2006**, *45*, 5527–5529.

(29) Crossley, S.; Faria, J.; Shen, M. D.; Resasco, D. E. Solid Nanoparticles that Catalyze Biofuel Upgrade Reactions at the Water/Oil Interface. *Science* **2010**, *327*, 68–72.

(30) Shan, Y. Y.; Yu, C.; Yang, J.; Dong, Q.; Fan, X. M.; Qiu, J. S. Thermodynamics-Stability Pickering Emulsion Configured with Carbon Nanotubes-Bridged Nanosheet-Shaped Layered Double Hydroxide for Selective Oxidation of Benzyl Alcohol. *ACS Appl. Mater. Interfaces* **2015**, *7*, 12203–12209.

(31) Pera-Titus, M.; Leclercq, L.; Clacens, J. M.; De Campo, F.; Nardello-Rataj, V. Pickering Interfacial Catalysis for Biphasic Systems: From Emulsion Design to Green Reactions. *Angew. Chem. Int. Ed.* **2015**, *54*, 2006–2021.

(32) Potier, J.; Menuel, S.; Monflier, E.; Hapiot, F. Synergetic Effect of Randomly Methylated β -Cyclodextrin and a Supramolecular Hydrogel in Rh-Catalyzed Hydroformylation of Higher Olefins. *ACS Catal.* **2014**, *4*, 2342–2346.

(33) Zhou, W. J.; Fang, L.; Fan, Z. Y.; Albela, B.; Laurent Bonneviot, L.; Campo, F. D.; Pera-Titus, M.; Clacens, J. M. Tunable Catalysts for Solvent-Free Biphasic Systems: Pickering Interfacial Catalysts over Amphiphilic Silica Nanoparticles. *J. Am. Chem. Soc.* **2014**, *136*, 4869–4872.

(34) Faria, J.; Ruiz, M. P.; Resasco, D. E. Phase-selective Catalysis in Emulsions Stabilized by Janus Silica-nanoparticles. *Adv. Synth. Catal.* **2010**, *352*, 2359–2364.

(35) Chen, Z. W.; Zhou, L.; Bing, W.; Zhang, Z. J.; Li, Z. H.; Ren, J. S.; Qu, X. G. Light Controlled Reversible Inversion of Nanophosphor-Stabilized Pickering Emulsions for Biphasic Enantioselective Biocatalysis. *J. Am. Chem. Soc.* **2014**, *136*, 7498–7504.

(36) Shi, J. F.; Wang, X. L.; Zhang, S. H.; Tang, L.; Jiang, Z. Y. Enzyme-Conjugated ZIF-8 Particles as Efficient and Stable Pickering Interfacial Biocatalysts for Biphasic Biocatalysis. *J. Mater. Chem. B* **2016**, *4*, 2654–2661.

(37) Song, Y.; Michaels, T. C. T.; Ma, Q. M.; Liu, Z.; Yuan, H.; Takayama, S.; Knowles, T. P. J.; Shum, H. C. Budding-like Division of All-aqueous Emulsion Droplets Modulated by Networks of Protein Nanofibrils. *Nat. Commun.* **2018**, *9*, 2110.

(38) Wang, Z. P.; van Oers, M. C.; Rutjes, F. P. J. T.; van Hest, J. C. Polymersome Colloidosomes for Enzyme Catalysis in a Biphasic System. *Angew. Chem. Int. Ed.* **2012**, *51*, 10746–10750.

(39) Sun, Z. Y.; Glebe, U.; Charan, H.; Böker, A.; Wu, C. Z. Enzyme-Polymer Conjugates as Robust Pickering Interfacial

Biocatalysts for Efficient Biotransformation and One-Pot Cascade Reactions. *Angew. Chem. Int. Ed.* **2018**, *57*, 13810–13814.

(40) Jiang, H.; Liu, L. D.; Li, Y. X.; Yin, S. W.; Ngai, T. Inverse Pickering Emulsion Stabilized by Binary Particles with Contrasting Characteristics and Functionality for Interfacial Biocatalysis. *ACS Appl. Mater. Interfaces* **2020**, *12*, 4989–4997.

(41) Liu, C. C.; Zhang, J. L.; Zheng, L. R.; Zhang, J.; Sang, X. X.; Kang, X. C.; Zhang, B. X.; Luo, T.; Tan, X. N.; Han, B. X. Metal–Organic Framework for Emulsifying Carbon Dioxide and Water. *Angew. Chem. Int., Ed.* **2016**, *55*, 11372–11376.

(42) Greydanus, B.; Schwartz, D. K.; Medlin, J. W. Controlling Catalyst-Phase Selectivity in Complex Mixtures with Amphiphilic Janus Particles. *ACS Appl. Mater. Interfaces* **2020**, *12*, 2338–2345.

(43) Bradley, L. C.; Stebe, K. J.; Lee, D. Clickable Janus Particles. *J. Am. Chem. Soc.* **2016**, *138*, 11437–11440.

(44) Zhang, M. J.; Tang, Z. Y.; Fu, W. Q.; Wang, W. Y.; Tan, R.; Yin, D. H. An Ionic Liquid-Functionalized Amphiphilic Janus Material as a Pickering Interfacial Catalyst for Asymmetric Sulfoxidation in Water. *Chem. Commun.* **2019**, *55*, 592–595.

(45) Liang, F. X.; Liu, B.; Cao, Z.; Yang, Z. Z. Janus Colloids toward Interfacial Engineering. *Langmuir* **2018**, *34*, 4123–4131.

(46) Kasuga, T.; Hiramatsu, M.; Hoson, A.; Sekino, T.; Niihara, K. Titania Nanotubes Prepared by Chemical Processing. *Adv. Mater.* **1999**, *11*, 1307–1311.

(47) Chen, Z. J.; Guan, Z. H.; Li, M. R.; Yang, Q. H.; Li, C. Enhancement of the Performance of a Platinum Nanocatalyst Confined within Carbon Nanotubes for Asymmetric Hydrogenation. *Angew. Chem. Int. Ed.* **2011**, *50*, 4913–4917.

(48) Liu, J.; He, S.; Li, C. M.; Wang, F.; Wei, M.; Evans, D. G.; Duan, X. Confined Synthesis of Ultrafine Ru–B Amorphous Alloy and its Catalytic Behavior toward Selective Hydrogenation of Benzene. *J. Mater. Chem. A* **2014**, *2*, 7570–7577.

(49) Narayan, S.; Muldoon, J.; Finn, M. G.; Fokin, V. V.; Kolb, H. C.; Sharpless, K. B. “On Water”: Unique Reactivity of Organic Compounds in Aqueous Suspension. *Angew. Chem. Int. Ed.* **2005**, *44*, 3275–3279.

(50) Song, C. E.; Park, S. J.; Hwang, I. S.; Jung, M. J.; Shim, S. Y.; Bae, H. Y.; Jung, J. Y. Hydrophobic Chirality Amplification in Confined Water Cages. *Nat. Commun.* **2019**, *10*, 851.

(51) Jung, Y.; Marcus, R. A. On the Theory of Organic Catalysis “On Water”. *J. Am. Chem. Soc.* **2007**, *129*, 5492–5502.

(52) Hibbitts, D. D.; Loveless, B. T.; Neurock, M.; Iglesia, E. Mechanistic Role of Water on the Rate and Selectivity of Fischer–Tropsch Synthesis on Ruthenium Catalysts. *Angew. Chem. Int. Ed.* **2013**, *52*, 12273–12278.

(53) Zhao, Z.; Bababrik, R.; Xue, W. H.; Li, Y. P.; Briggs, N. M.; Nguyen, D. T.; Nguyen, U.; Crossley, S. P.; Wang, S. W.; Wang, B.; Resasco, D. E. Solvent-Mediated Charge Separation Drives Alternative Hydrogenation Path of Furans in Liquid Water. *Nat. Catal.* **2019**, *2*, 431–436.

(54) Li, G. N.; Wang, B.; Resasco, D. E. Water-Mediated Heterogeneously Catalyzed Reactions. *ACS Catal.* **2020**, *10*, 1294–1309.

(55) Michel, C.; Gallezot, P. Why is Ruthenium an Efficient Catalyst for the Aqueous-Phase Hydrogenation of Biosourced Carbonyl Compounds? *ACS Catal.* **2015**, *5*, 4130–4132.

(56) Zhang, K. L.; Yang, Y. P.; Liu, H.; Liu, Q. X.; Lv, J. L.; Zhou, H. F. Enantioselective Synthesis of 2-Hydroxyalkyl Diarylphosphinates by Ruthenium-Catalyzed Asymmetric Transfer Hydrogenation. *Adv. Synth. Catal.* **2019**, *361*, 4106–4110.

(57) Bai, L.; Greca, L. G.; Xiang, W. C.; Lehtonen, J.; Huan, S. Q.; Nugroho, R. W. N.; Tardy, B. L.; Rojas, O. J. Adsorption and Assembly of Cellulosic and Lignin Colloids at oil/water Interfaces. *Langmuir* **2019**, *35*, 571–588.

(58) Kalashnikova, I.; Bizot, H.; Bertocini, P.; Cathala, B.; Capron, I. Cellulosic Nanorods of Various Aspect ratios for Oil in Water Pickering Emulsions. *Soft Matter* **2013**, *9*, 952–959.

(59) Bourikas, K.; Stylidi, M.; Kondarides, D. I.; Verykios, X. E. Adsorption of Acid Orange 7 on the Surface of Titanium Dioxide. *Langmuir* **2005**, *21*, 9222–9230.

(60) Feng, T.; Hoagland, D. A.; Russell, T. P. Assembly of Acid-Functionalized Single-Walled Carbon Nanotubes at Oil/Water Interfaces. *Langmuir* **2014**, *30*, 1072–1079.

(61) Chaudhari, R. V.; Bhanage, B. M.; Deshpande, R. M.; Delmas, H. Enhancement of Interfacial Catalysis in a Biphasic System Using Catalyst-Binding Ligands. *Nature* **1995**, *373*, 501–503.

(62) Sieffert, N.; Wipff, G. Importance of Interfacial Adsorption in the Biphasic Hydroformylation of Higher Olefins Promoted by Cyclodextrins: A Molecular Dynamics Study at the Decene/Water Interface. *Chem. Eur. J.* **2007**, *13*, 1978–1990.

(63) Lee, J. K.; Samanta, D.; Nam, H. G.; Zare, R. N. Micrometer-Sized Water Droplets Induce Spontaneous Reduction. *J. Am. Chem. Soc.* **2019**, *141*, 10585–10589.

(64) Mishra, H.; Enami, S.; Nielsen, R. J.; Stewart, L. A.; Hoffmann, M. R.; Goddard, W. A. III; Agustin, J.; Colussi, A. J. Brønsted basicity of the Air–Water Interface. *Proc. Natl. Acad. Sci. U. S. A.* **2012**, *109*, 18679–18683.

For Table of Contents Only

